Available online at www.sciencedirect.com
SCIENCE DIRECT®
International Journal of Multiphase Flow 30 (2004) 675–696
International Journal of Multiphase Flow
www.elsevier.com/locate/ijmulflow

A geometric approach for predicting vertical stationary profiles of weakly inertial advecting-diffusing particles in closed incompressible flows

Stefano Cerbelli [a,*], Giuseppina Montante [b], Franco Grisafi [c]

[a] *Dipartimento di Ingegneria Chimica, Università di Roma "La Sapienza", via Eudossiana 18, 00184 Roma, Italy*
[b] *Dipartimento di Ingegneria Chimica, Mineraria e delle Tecnologie Ambientali, Università degli studi di Bologna, viale Risorgimento 2, 40136 Bologna, Italy*
[c] *Dipartimento di Ingegneria Chimica dei Processi e Materiali, Università degli studi di Palermo, viale delle Scienze, 90128 Palermo, Italy*

Received 24 March 2003; received in revised form 24 March 2004

Abstract

Mixing of weakly inertial particles in closed flows is often addressed by considering individual particles as passive advecting-diffusing tracers, subjected to an additional settling velocity resulting from body forces (e.g. gravity). We show that the qualitative and quantitative features of the vertical particle distribution (i.e. the horizontal cross-sectional averages of particle concentration) can be predicted from the structure of the flow resulting from the superposition of the stirring field and the settling velocity. The prediction is based upon the observation that the resulting flow can be divided into two nonoverlapping regions, namely trajectories that are confined within the mixing space (recirculation loops), and trajectories that cross the mixing space. The spatial extent of these regions is exploited to define an effective vertical convective velocity entering the one-dimensional lumped model. Model two-dimensional flows possessing different flow patterns are used to illustrate the proposed estimate for effective velocity. A CFD-computed three-dimensional turbulent flow inside a baffled stirred vessel is used as a benchmark test to assess the model performance in typical industrial flows.

* Corresponding author. Tel.: +1139-0644585609; fax: +1139-0644585451.
E-mail address: stefano@giona.ing.uniroma1.it (S. Cerbelli).

0301-9322/$ - see front matter © 2004 Elsevier Ltd. All rights reserved.
doi:10.1016/j.ijmultiphaseflow.2004.04.001

1. Introduction

Homogenization of a dispersed phase within a flowing continuum has been the object of considerable attention in the past, under both fundamental (Shirolkar et al., 1996), numerical (Loth, 2000), and practical (Harnby et al., 1997) viewpoints.

The manifold of systems that can be described within this conceptual framework encompasses natural phenomena, e.g. spreading of impurities in the atmosphere (Lamb, 1980), as well as man-made applications such as combustion of solid particles and liquid sprays (Shirolkar et al., 1996), electrostatic precipitators (Leonard et al., 1980), etc.

The wide range of length and temporal scales involved in these systems makes the phenomenology of two-phase dispersion rich and diversified. At the same time, it forces the modelist to choose among several possible approaches in order to single out the simplest method that can explain the phenomenon of interest.

The most general (Lagrangian) approach consists of regarding the dispersed phase as composed by individual particles subjected to body forces (e.g. gravity, electrostatic) and exchanging surface (drag) forces arising from thermal and turbulent fluctuations as well as from the mean flow of the surrounding fluid (see, e.g., Kudrna et al., 1986; Reeks, 1983; a derivation of all the force terms applied by a moving continuum upon a single spherical particle is discussed in Maxey and Riley, 1983). For a single particle, this translates into considering six nonlinear equations that include deterministic terms from the mean field, and stochastic terms from the thermal and velocity fluctuations (Langevin equation). The Eulerian counterpart of this approach is provided by the Fokker–Planck equation governing the evolution of the probability density function $\mathscr{P}(\mathbf{x}, \mathbf{v}, t)$, expressing the probability that a given particle passes through the position $\mathbf{x}$ with velocity $\mathbf{v}$ at the time t (Zaichik, 1997). However, the direct solution of either the Langevin or the Fokker–Planck equation is generally not attainable by simple methods when real world systems are to be dealt with.

A widely used approximation that applies when low mass loadings of small-sized particle are involved consists of assuming that the particle velocity is the sum of the local fluid velocity, say $\mathbf{w}(\mathbf{x}, t)$, plus an inertial contribution, $\mathbf{v}_g$, that arises as a consequence of body forces (e.g. gravity or, for charged particles, electrostatic potential). Also, it is assumed that the velocity field, $\mathbf{w}$, of the carrier flow is not modified by the presence of the dispersed phase. A quantitative criterion for establishing the validity of this assumption is that it must be $\varepsilon\rho_p \ll (1-\varepsilon)\rho_f$, where ε is the volume fraction of particles, and ρ_p, ρ_f are the particle and carrier fluid densities, respectively (Johansen, 1991).

This approximation, usually referred to as the settling velocity model (SVM), has proved useful in addressing quantitatively a number of industrial applications, such as steady-state distribution (Micale et al., 2000) and dynamics of dispersion (Montante et al., 2002) of small particles in stirred vessels, as well as deposition of charged particles in electrostatic precipitators (Leonard et al., 1980).

The Eulerian description of the particle concentration $c(\mathbf{x}, t)$ (also referred to as particle number density) is governed by the partial differential equation (PDE)

$$\frac{\partial c}{\partial t} = -(\mathbf{w} + \mathbf{v}_g) \cdot \nabla c + \nabla \cdot [\mathscr{D}_E \nabla c], \tag{1}$$

where $\mathbf{v}_g$ can be regarded as a constant vector field in most cases (e.g. gravity or electrostatic field). The system effective diffusivity, $\mathscr{D}_E$, results from both thermal and turbulent fluctuations of the carrier phase, and is represented, in the most general case, by a spatially-dependent positive definite symmetric tensor [1].

In many systems of interest (e.g. stirred slurry reactors), the carrier phase is a liquid flowing within a bounded domain, say Ω. Therefore, the velocity field $\mathbf{w}$ entering Eq. (1) is incompressible, i.e. $\nabla \cdot \mathbf{w} = 0$, and it results $\mathbf{w} = 0$ on the boundary $\partial\Omega$ of the mixing space Ω.

In applications and experiments, it is often sufficient to determine the steady-state average particle concentration $C(z)$ along the direction of the settling bias (i.e. $C(z)$ is the average of the local concentration $c(\mathbf{x})$ onto a cross-section of the stirring device normal to the settling bias).

In this framework, the most simplified modeling consists of regarding Eq. (1) as defined on a one-dimensional interval spanning the equipment height, say L_Z. However, as it is immediate to verify, this simplification cannot account for the presence of the stirring field. Indeed, by the fact that the flow is incompressible and that the boundaries are impermeable, one obtains that $\mathbf{w}(\mathbf{x}, t) = w_z(z, t)$ should vanish identically in the entire interval $[0, L_z]$ (i.e. any incompressible one-dimensional flow is necessarily constant), thus yielding the partial differential model

$$\frac{\partial C}{\partial t} = -v_g \frac{\partial C}{\partial z} + \mathscr{D}_E \frac{\partial^2 C}{\partial z^2}, \tag{2}$$

equipped with the zero net flux boundary conditions, $v_g C - \mathscr{D}_E \partial C/\partial z = 0$ at the boundaries $z = 0$ and L_z. Thus, the steady-state profile associated with the one-dimensional setting of the SVM is given by the exponential $C(z) = Pe \exp[-Pez]/(1 - \exp[-PeL_Z])$, where $Pe = v_g L_Z / D_E$.

This approach has been mainly used to determine the parameters v_g and $\mathscr{D}_E$ from regression of experimental data (Nocentini et al., 2002; Magelli et al., 1990; Barresi and Baldi, 1987). It was noted, however, that the vertical concentration profiles determined experimentally showed a complex dependence with the z-coordinate, with staircase-like "humps" superimposed to the exponential backbone. This deviation from the idealized exponential profile was attributed to interactions between the particles and the carrier flow turbulence that had not been accounted for in the model (Pinelli et al., 2001).

In point of fact, a number of studies focusing on the influence of the mean flow upon particle distribution showed that nonexponential profiles can arise even in the absence of particle–turbulence interaction modeling, as soon as a higher dimensional setting for Eq. (1) is considered (Brucato et al., 1991; Mann, 1986; Micale et al., 2000; Brucato et al., 1997). In other words, a spatially nonuniform two or three-dimensional velocity field $\mathbf{w}(\mathbf{x}, t)$ can yield vertical concentration profiles qualitatively and quantitatively analogous to those observed experimentally.

The action of a two or three-dimensional flow on the steady-state vertical profile can be envisioned as the result of an effective velocity $v_E(z)$ which arises from the correlations between the vertical flow $w_z(\mathbf{x}, t)$ and the structure of the concentration field $c(\mathbf{x}, t)$ onto the cross-section at the generic height z (see Section 3 for details). In this work, we propose a simple model to estimate

[1] In the case of a wall-bounded turbulent flow of the continuous fluid phase, the spatial dependence as well as the tensor character of the diffusivity is a direct consequence of the spatially distributed structure of turbulence intensities (see Section 2).

the effective velocity $v_E(z)$ based solely on the knowledge of the stirring flow $\mathbf{w}$ and the settling bias v_g. The model is fully predictive in that contains no adjustable parameters, and stems from the observation that the flow resulting from the superposition of $\mathbf{w}$ and the settling bias $v_g\mathbf{e}_z$ can be decomposed into two disjoint regions, namely a collection of recirculation loops, and an inflowing–outflowing flux tube whose horizontal cross-section varies with the z-coordinate. Based on this observation, a simple relationship between the vertical effective velocity and the geometry of the flux tube is proposed.

The model is illustrated by using examples of steady two-dimensional flows, namely a model incompressible flow stemming from a sinusoidal streamfunction, and the cavity flow system, i.e. the physically realizable Stokesian flow occurring in a rectangular cavity with one or more walls moving at constant speed. The case of a CFD computed turbulent flow inside a baffled stirred vessel is thus used as a benchmark test to assess the validity of the model.

2. Statement of the problem and flow systems

In this section, we introduce three models of steady two-dimensional incompressible flows defined within a square box $\Omega = \{(x,y)|\ 0 \leqslant x \leqslant L,\ 0 \leqslant y \leqslant L\}$, in order to analyze the relationships between the qualitative features of the stirring flow and the steady-state particle distribution. As the flows are incompressible, the velocity field $\mathbf{w}(x,y) = (w_x(x,y), w_y(x,y))$ is defined via its streamfunction $\Psi(x,y)$ as $(w_x, w_y) = (\partial\Psi/\partial y,\ -\partial\Psi/\partial x)$.

The first flow system, referred to as Model **A** stems from the streamfunction

$$\Psi_A = \sin(\pi x/L)\sin(2\pi y/L). \tag{3}$$

Although the corresponding velocity field is not a solution of a Navier–Stokes boundary value problem, cellular streamfunctions of the type given in Eq. (3) are a standard tool widely used in the Literature in order to assess the interaction between advection and diffusion in the transport of scalar as well as vector quantities (Fannjiang and Papanicolau, 1994; Childress and Soward, 1989).

The other class of model flows considered consists of physically realizable creeping flows resulting from the steady motion of the walls delimiting the rectangular cavity (cavity flow system (CF)). The CF is obtained as the solution of the Stokesian boundary value problem (BVP) specified by the PDE involving the streamfunction Ψ, $\Delta^2\Psi = 0$ in Ω (where Δ^2 denotes the biharmonic operator), and the boundary conditions $\partial\Psi/\partial n = V_w$ and $\partial\Psi/\partial\tau = 0$ on the boundary $\partial\Omega$ of the flow domain, where n and τ are the local normal and tangent direction to the cavity edges, and V_w is the wall velocity (see, e.g., Ottino, 1989). The first boundary condition corresponds to usual the no-slip condition, whereas the second (involving the tangential derivative) expresses impermeability at the domain walls.

Notwithstanding the linearity of the BVP and the simple structure of the flow domain, a closed-form solution for the stream function is not available, and numerical approaches must be used to determine the flow within the cavity. We used a relaxation finite difference scheme in order to obtain the solution Ψ onto a square grid of 71×71 points uniformly distributed in the square cavity. We considered two sets of boundary conditions, henceforth referred to as Model **B** and

Model **C**, corresponding to the motion of top and bottom walls, and top and right walls, respectively.

Fig. 1 shows the contour levels of the three model systems. For the cavity flows Model **B** and **C**, the arrows in the figure indicate the direction of motion of the walls.

Let us make Eq. (1) dimensionless by introducing the rescaled variables

$$\begin{aligned} &\tilde{x} = \frac{x}{L} \quad \tilde{y} = \frac{y}{L} \quad \theta = \frac{t v_g}{L}, \quad \tilde{c} = \frac{c}{C_{ref}} \\ &\hat{\mathbf{v}} = \frac{\mathbf{w}}{V} \quad \beta = \frac{V}{v_g}, \end{aligned} \tag{4}$$

where V is the L_2 norm of the velocity field, $V = \left[\int_\Omega \mathbf{w}\cdot\mathbf{w}\,\mathrm{d}x\,\mathrm{d}y\right]^{1/2}$, v_g is the magnitude of the settling velocity vector, and C_{ref} is a reference concentration, that can be chosen in order to make the overall solid amount equal to unity, $\int_\Omega \tilde{c}(\tilde{x},\tilde{y},\theta)\,\mathrm{d}\tilde{x}\,\mathrm{d}\tilde{y} = 1$. The parameter β, referred to as the *flow-to-settling ratio*, represents the ratio of the L_2 norm of the stirring flow to the particle settling velocity. By assuming that the settling velocity is directed vertically, $\mathbf{v}_g = (0, -v_g)$, and that the effective diffusivity $\mathscr{D}_E$ can be considered constant throughout the mixing space, the dimensionless formulation of the SVM writes

$$\frac{\partial \tilde{c}}{\partial \theta} = -\beta\ \mathbf{v}\cdot\nabla\tilde{c} + \frac{\partial \tilde{c}}{\partial \tilde{y}} + \frac{1}{Pe}\nabla^2\tilde{c}, \tag{5}$$

where $Pe = v_g L/\mathscr{D}_E$ is the Peclet number referred to the particle settling velocity v_g.

In order to assess the range of applicability of the SVM to experimental or industrial flows, it is important to stress out the physical meaning of the effective diffusivity parameter, $\mathscr{D}_E = \mathscr{D}_M + \mathscr{D}_T$, which accounts for both thermal and velocity fluctuations of the carrier flow through the molecular and turbulent contribution, $\mathscr{D}_M$ and $\mathscr{D}_T$, respectively. While there are models available in the literature that predict the thermal diffusivity coefficient $\mathscr{D}_M$ with reasonable accuracy (see, e.g. Young and Leeming, 1997), the estimate of $\mathscr{D}_T$ is generally difficult, even in the case where the spatial structure of turbulent intensity of the carrier flow is known with a certain accuracy. The two main reasons that make the estimate difficult are: (i) the nonhomogeneous nonisotropic structure of turbulence in the presence of solid walls, which implies that the dispersion caused by turbulent fluctuations be represented by a spatially-dependent

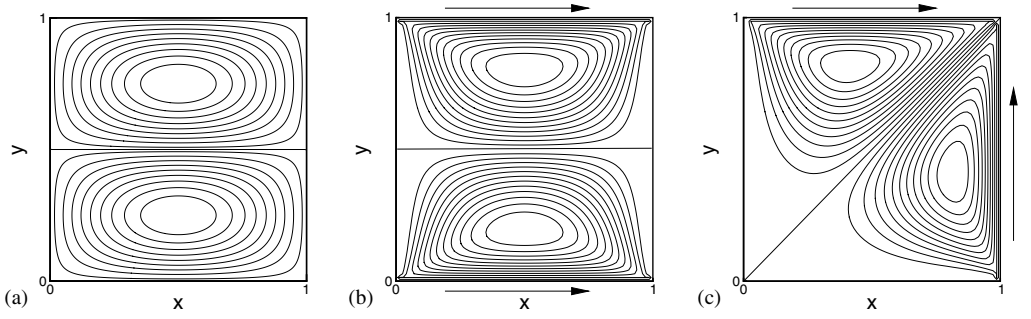

Fig. 1. Streamlines for Model **A** (a); Model **B** (b); Model **C** (c) flows. The arrows in panels (b) and (c) indicate the direction of motion of the walls.

tensor quantity, (ii) the presence of particle inertia, which makes trajectories of solid particles deviate from those of passive tracers moving along with the carrier flow; this implies that in principle $\mathscr{D}_T$ could depend on particle inertia and cannot be considered as a characteristic of the carrier flow alone. In practice, the deviation from the behavior of a passive tracer caused by particle inertia is important only in nonhomogeneous turbulence (see Young and Leeming, 1997, and references therein), which, however, is the case of most flows of practical interest. In any case, when dealing with real world mixers operating in turbulent regime, determining the spatial dependence of the effective diffusivity tensor results impractical, and options are either to regard *Pe* as a lumped parameter to be determined by best fit of experimental data, or to assume the turbulent contribution to particle effective diffusivity $\mathscr{D}_T$ equal to that of the carrier flow (Pinelli et al., 2001). As in this article we are mainly interested in assessing the impact of the mean flow on particle distribution at steady-state, the value $Pe = 4$ was chosen as representative of typical experimental conditions (see, e.g., Pinelli et al., 2001; Magelli et al., 1990).

Going back to our flow models, since, by definition, the normal component of velocity field $\mathbf{v}$ vanishes at the boundary of the cavity, the boundary conditions associated with Eq. (5) are:

$$\left.\frac{\partial \tilde{c}}{\partial \tilde{x}}\right|_{\tilde{x}=0,1} = 0, \quad \tilde{c} + \frac{1}{Pe}\left.\frac{\partial \tilde{c}}{\partial \tilde{y}}\right|_{\tilde{y}=0,1} = 0. \tag{6}$$

Owing to the presence of the stirring field $\mathbf{v}(\tilde{x}, \tilde{y})$, the solution of Eq. (5) must be approached numerically. Starting from a uniform initial distribution of particles $\tilde{c}(\tilde{x}, \tilde{y}, 0) = 1$, we used an explicit finite volume (FV) scheme in order to obtain the time-dependent concentration fields. For the CF system, the same grid used for obtaining the solution of the cavity flow problem was used to define the volume elements of the FV discretization. With this choice, the convective fluxes across the cell faces can be directly computed by the nodal values of the streamfunction, with no need for interpolation or numerical differentiation of the streamfunction. In passing, we remark that the use of the streamfunction for defining the convective fluxes of the FV method allows to preserve the incompressible nature of the flow even for the discretized form of Eq. (5). The parameter β was chosen in the range $\beta \in [1, 256]$. As in the limit $v_g \to 0$, (i.e. $\beta \to \infty$) particles behave as passive tracers, it is expected that increasing the parameter β will result in stationary concentration fields that become more and more homogeneous. On the other hand, for $\beta \to 0$ the steady-state concentration can be obtained explicitly,

$$\tilde{c}(\tilde{x}, \tilde{y}, \theta \to \infty) = Pe \exp(-Pe\ \tilde{y})/(1 - \exp(-Pe)). \tag{7}$$

Fig. 2 shows the steady-state particle distribution for Model **A** flow and Model **B** flow at $\beta = 4$ and 128, respectively. The comparison shows that, as expected, higher β-values correspond to more efficient homogenization (note that the range of concentration values is different in the four panels). Also, the structure of the concentration field for the higher β-value shows two plateau that resemble closely the structure of the two vortices of Model **A** flow and Model **B** flow. In both cases, the steepest concentration gradient is localized in the region between the two vortices.

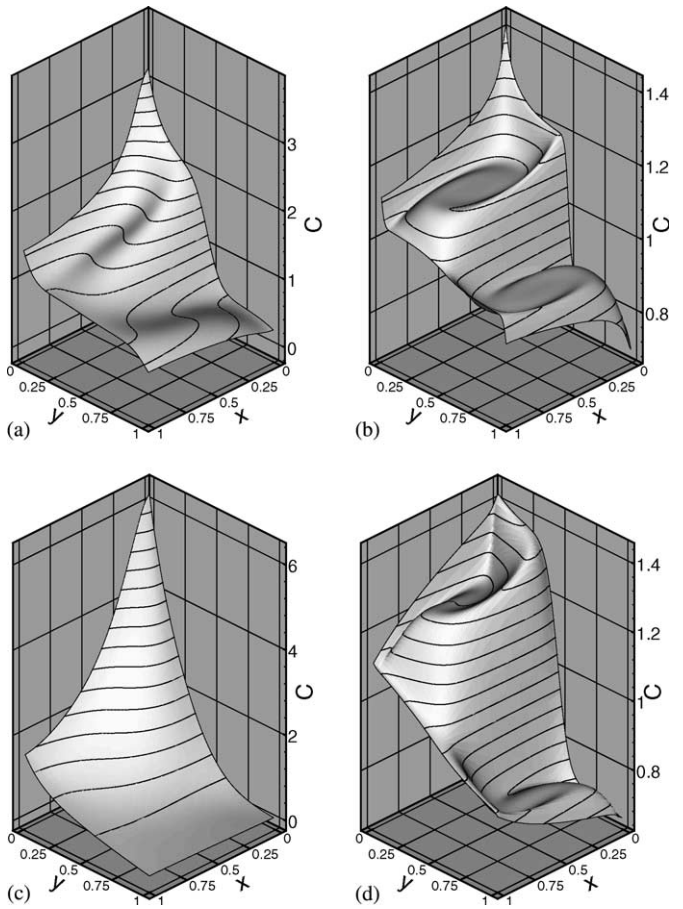

Fig. 2. Two-dimensional concentration fields at steady-state at $Pe = 4$. (a) Model **A** flow with $\beta = 4$; (b) Model **A** flow with $\beta = 128$; (c) Model **B** flow with $\beta = 4$; (d) Model **B** flow with $\beta = 128$.

3. One-dimensional averaged profiles

As discussed in the Introduction, in many applications and experiments the knowledge of the cross-section averaged concentration $\overline{C}$ is sought. In our case, $\overline{C}(\tilde{y}, \theta)$ is defined as

$$\overline{C}(\tilde{y}, \theta) = \int_0^1 \tilde{c}(\tilde{x}, \tilde{y}, \theta)\, \mathrm{d}\tilde{x}. \tag{8}$$

The equation defining $\overline{C}$ can be obtained by integrating both sides of Eq. (5) onto the horizontal cross-section at the generic height y. One obtains

$$\frac{\partial \overline{C}}{\partial \theta} = \underbrace{-\beta \int_0^1 \frac{\partial (v_x \tilde{c})}{\partial \tilde{x}}\, \mathrm{d}\tilde{x}}_{I_1} \underbrace{-\beta \frac{\partial}{\partial \tilde{y}} \int_0^1 v_y \tilde{c}\, \mathrm{d}\tilde{x}}_{I_2} + \frac{\partial \overline{C}}{\partial \tilde{y}} + \frac{1}{Pe} \underbrace{\int_0^1 \frac{\partial^2 \tilde{c}}{\partial \tilde{x}^2}\, \mathrm{d}\tilde{x}}_{I_3} + \frac{1}{Pe} \frac{\partial^2 \overline{C}}{\partial \tilde{y}^2}. \tag{9}$$

As it is immediate to verify, the integral terms I_1 and I_3 vanish at any $\tilde{y}$, the first because of the impermeability condition of the stirring flow at the vertical walls, the second because of the zero net flux boundary conditions expressed by Eq. (6). Thus, one is left with an equation in $\overline{C}$ that is identical to that associated with a one-dimensional system (see Eq. (2)), but for the presence of the integral term I_2, which depends on the correlations between the particle concentration and the vertical component of the stirring flow along the horizontal cross-section. By defining the *effective velocity* $v_E(\tilde{y})$ through

$$v_E(\tilde{y})\overline{C}(\tilde{y},\theta) = \int_0^1 v_y(\tilde{x},\tilde{y})\ \tilde{c}(\tilde{x},\tilde{y},\theta)\,\mathrm{d}\tilde{x}, \tag{10}$$

one obtains that $\overline{C}$ must satisfy the following equation

$$\frac{\partial \overline{C}}{\partial \theta} = -\beta \frac{\partial (v_E(\tilde{y})\overline{C})}{\partial \tilde{y}} + \frac{\partial \overline{C}}{\partial \tilde{y}} + \frac{1}{Pe}\frac{\partial^2 \overline{C}}{\partial \tilde{y}^2}, \tag{11}$$

with the boundary conditions, $\overline{C} - (1/Pe)\,\partial\overline{C}/\partial\tilde{y} = 0$ at $\tilde{y} = 0$ and 1. It should be noted that a nonzero value of the effective velocity is strictly related to a variable concentration profile along the horizontal coordinate $\tilde{x}$. Indeed, were the concentration along the horizontal cross-section uniform, i.e. $\tilde{c}(\tilde{x},\tilde{y},\theta) = c_0$ when $\tilde{y}, \theta =$ constant and $0 < \tilde{x} < 1$, then the integral term at the RHS of Eq. (10) would vanish

$$\int_0^1 v_y(\tilde{x},\tilde{y})\tilde{c}(\tilde{x},\tilde{y},\theta)\,\mathrm{d}\tilde{x} = c_0 \int_0^1 v_y(\tilde{x},\tilde{y})\,\mathrm{d}\tilde{x} = 0 \tag{12}$$

because of the incompressible nature of the stirring flow and of the impermeability of the domain walls. Thus, in order to determine the cross-section averaged profiles, a "constitutive" closure equation (e.g. based on physical arguments) for the effective velocity must be provided. Once the structural form of $v_E(\tilde{y})$ has been established, the steady-state profile for the average concentration can be obtained by quadratures as

$$\overline{C}_{ss} = A \exp\left\{ -Pe\left[\tilde{y} - \beta \int_0^{\tilde{y}} v_E(s)\,\mathrm{d}s\right]\right\}, \tag{13}$$

where $A = 1/\int_0^1 \exp\left\{-Pe[\tilde{y} - \beta\int_0^{\tilde{y}} v_E(s)\,\mathrm{d}s]\right\}\mathrm{d}\tilde{y}$.

Fig. 3 shows the average steady-state concentration profiles $\overline{C}_{ss}(\tilde{y})$ (continuous lines), and the effective velocity $v_E(\tilde{y})$ (dotted lines) computed a posteriori from the data showed in Fig. 2(c) and (d). By Eq. (13), the effective velocity is given by $\beta v_E(\tilde{y}) = 1 + (1/Pe)\,\mathrm{d}(\log[\overline{C}_{ss}(\tilde{y})])/\mathrm{d}\tilde{y}$. Thus, once the vertical concentration profile has been obtained by averaging onto the horizontal cross-section the two-dimensional concentration field, the "true" effective velocity can be computed by numerical differentiating the profile itself. In the reminder, we refer to this quantity as the *computed effective velocity*, as opposed to the estimated effective velocity provided by Eq. (15).

The case $\beta = 4$ (curve A) shows a concentration profile very similar to the ideal exponential decay that pertains to a system without stirring, whereas at $\beta = 128$, the particle distribution is nearly uniform, with concentration gradients localized next to the walls and at the boundary of the two counter rotating vortices (compare with Fig. 1). Accordingly, the effective velocity profile

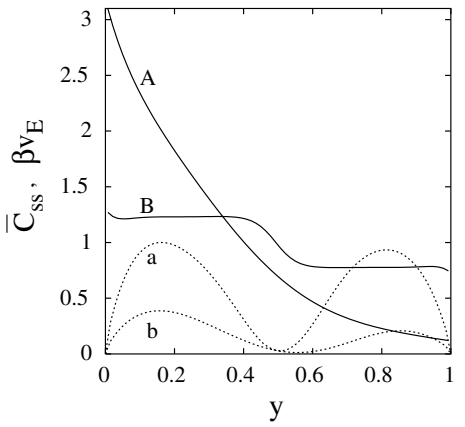

Fig. 3. Continuous lines: cross-section averaged concentration profile $\overline{C}_{ss}(\tilde{y})$ for Model **A** flow at $Pe = 4$ and $\beta = 4$ (curve A) and $\beta = 128$ (curve B) computed by direct numerical FV simulation. Dotted lines: profiles of the corresponding effective velocity $\beta v_E(\tilde{y})$, (curve (a) $\beta = 4$, curve (b) $\beta = 128$).

is more pronounced at the highest β value, thus indicating an efficient action of the stirring field in uniformly distributing particles throughout the mixing space.

4. Closure approximation for the effective velocity

The results of FV direct numerical simulation discussed in the previous section showed that there exists a correlation between the structure of the stirring flow and the profile of effective velocity entering the one-dimensional lumped model expressed by Eq. (11). However, the intensity of the effective velocity is clearly related to the value of the flow-to-settling ratio parameter β. This suggests that an estimate of the settling velocity profile could be based on the flow

$$\mathbf{u}(\tilde{x}, \tilde{y}; \beta) = \beta \mathbf{v} - \mathbf{e}_y, \tag{14}$$

resulting from the superposition of the stirring flow $\beta\mathbf{v}$, and $-\mathbf{e}_y$ representing the (dimensionless) contribution of the settling bias. It can be noted that, by the definition expressed by Eq. (14), the resulting flow $\mathbf{u}(\tilde{x}, \tilde{y}; \beta)$ can also be expressed in terms of the streamfunction $\Phi = \beta\Psi + \tilde{x}$ (Ψ being the streamfunction of the stirring flow $\mathbf{v}$) as $\mathbf{u} = (u_x, u_y) = (\partial\Phi/\partial\tilde{y}, -\partial\Phi/\partial\tilde{x})$.

Fig. 4(a) and (b) show the structure of $\mathbf{u}$ for Model **A** flow at $\beta = 1$ and 8, respectively.

By the fact that the flow is incompressible, (almost all) the trajectories of passively advected particles that start at the upper wall must intersect the lower wall. Thus, they define an inflowing–outflowing flux tube that crosses the mixing space. The remaining two lobe-shaped regions bounded by the thick lines are recirculation loops that exchange particles with the flux tube only by diffusion mechanism.

The spatial extent of the recirculation vortices becomes bigger and bigger as the flow-to-settling ratio β increases. Due to the underlying symmetries of the stirring flow Model **A**, the structure of the flux tube is particularly simple, with the inflowing–outflowing streamlines always possessing a negative y velocity component i.e. the $\tilde{y}$-component of the resulting flow $\mathbf{u}$ along any of the

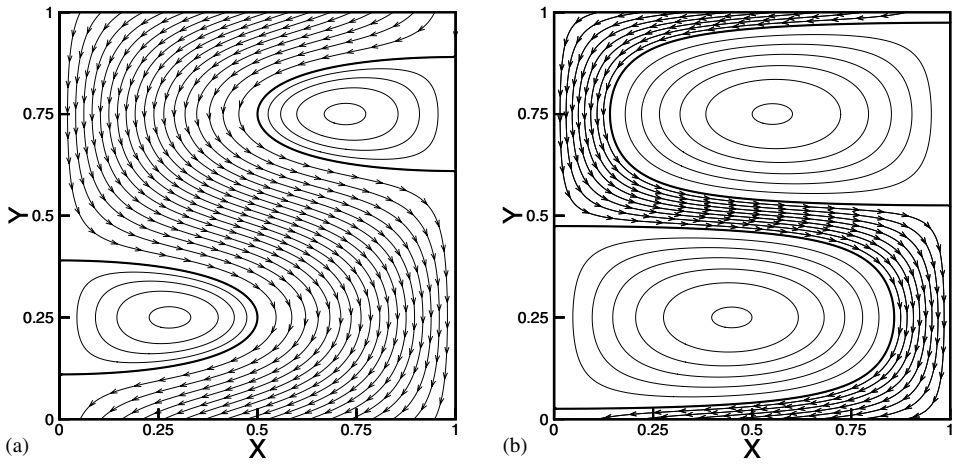

Fig. 4. Flow structure for Model **A** flow at $\beta = 1$ (a) and $\beta = 8$ (b). The flow domain is composed by an inflowing–outflowing flux tube and two recirculation vortices. The thick lines denote the boundaries of the flux tube.

streamlines composing the flux tube is always directed as the settling bias. This property is by no means general, and remarkably complex structures of the flux tube can arise when stirring flows that lack the elementary symmetries of Model **A** are considered.

Next, we analyze in more detail this simple situation in order to derive some connections between the geometric structure of the flux tube and the profile of the effective velocity. Let us thus consider a horizontal cross-section $\Sigma(\tilde{y}_0)$ of the flow domain at a generic height $\tilde{y}_0$. Denote with $\sigma(\tilde{y}_0)$ the set of points of $\Sigma(\tilde{y}_0)$ that belong to the inflowing–outflowing flux tube, as depicted in Fig. 5. Depending on the value of $\tilde{y}_0$, σ can be either strictly contained in, or coincident with, the

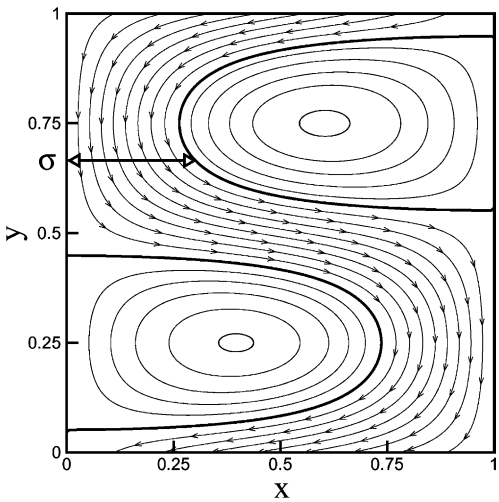

Fig. 5. The inflowing–outflowing flux tube cross-section for Model **A** at $\beta = 2$. In the case of model **A** flow $\sigma(\tilde{y}) = \sigma_{-}(\tilde{y})$ for any $\tilde{y}$ and any β.

system cross-section Σ. By comparing Figs. 5 and 3, it can be observed that the measure $\mu(\sigma(\tilde{y}))$ the flux tube cross-section $\sigma(\tilde{y})$ displays a strong relation with the vertical velocity $v_{0v} = 1 - \beta v_E$. In particular, at heights next to the center of recirculation vortices, the flux tube shrinks down to its minimum width, whereas the effective velocity shows local maxima. Conversely, at $\tilde{y} \sim 1/2$, the effective velocity is nearly vanishing, while the flux tube cross-section coincides with the system cross-section.

Thus, in the case of Model **A** flow, a simple estimate of the effective velocity could be expressed in terms of the geometric features of the stirring flow as the ratio of the flux tube cross-section to the overall cross-section of the system, i.e. $1 - \beta v_E = \mu(\sigma(\tilde{y}))/\mu(\Sigma)$, where $\mu(\Sigma)$ is identically unity since the flow is defined in a unit square box. In other words, the lumped one-dimensional model is constructed by assuming that while the entire cross-section is available to diffusional particle transport, the convective particle transport is effective only inside the inflowing–outflowing flux tube. As a consequence, the magnitude of the overall vertical velocity $\beta v_E - 1$ is reduced by a factor $\mu(\sigma(\tilde{y}))/\mu(\Sigma)$, which results upperbounded by unity. Thus, the dimensional overall vertical velocity predicted by this closure approximation is always oriented as the settling bias, and its magnitude results less than, or at most equal to, the settling velocity.

As observed above, more complex structures of the flux tube can arise when the stirring flow lacks the simple symmetries of Model **A** flow. In particular the property by which the vertical velocity component is everywhere oriented as the forcing bias does not hold true for a generic stirring flow. In the general case, the flux tube cross-section σ can be decomposed into two non-overlapping sets, $\sigma_-(\tilde{y})$, and $\sigma_+(\tilde{y})$, representing the subsets of σ where the vertical velocity of the resulting flow is oriented in the same direction or in the opposite direction with respect to the settling bias, respectively. In the framework of the physical picture described above, the effective cross-section of the convective flux tube is set equal to the difference $\sigma_-(\tilde{y}) - \sigma_+(\tilde{y})$, which is assumed to represent the net contribution to the convective transport along the direction of the settling bias.

Thus, the closure approximation for a generic flow can be written as

$$\beta v_E(\tilde{y}) = 1 - \frac{\mu(\sigma_-(\tilde{y})) - \mu(\sigma_+(\tilde{y}))}{\mu(\Sigma(\tilde{y}))}. \tag{15}$$

Let us first examine the consistency of this estimate in the limit $\beta \to 0$, and $\beta \to \infty$. At $\beta = 0$, the resulting flow $\mathbf{u}$ coincides with the constant settling bias $-\mathbf{e}_y$. Thus, $\mu(\sigma_+(\tilde{y})) = 0$, $\mu(\sigma_-(\tilde{y})) = \mu(\Sigma) = 1$ at any $\tilde{y}$. Therefore, the effective velocity is everywhere zero, and the exponential steady-state profile is recovered.

At large β-values, the spatial extent of the diffusive recirculation vortices invades all of the available space at almost all $\tilde{y}$, thus yielding $\beta v_E(\tilde{y}) \to 1$. In this situation, the overall vertical velocity vanishes (i.e. the modulus of the effective velocity is unity), and the steady-state profile approaches a flat (i.e. homogeneous) distribution.

Fig. 6(a) and (b) shows the steady-state profiles obtained from direct numerical FV simulation of Eq. (5), and those predicted by Eq. (13) with v_E given by Eq. (15), respectively, for the case of Model **A** flow. In both panels, the arrows indicate increasing values of β. The qualitative agreement between computed and predicted profiles indicate that, at least for the specific case of Model **A** flow, the proposed estimate for the effective velocity captures the basic mechanisms of interaction between particle dispersion and the stirring action of the resulting flow.

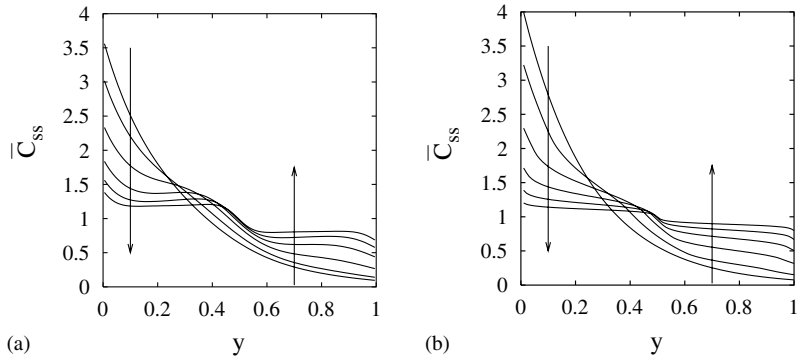

Fig. 6. Steady-state profiles, $\overline{C}_{ss}(\tilde{y})$, for model **A** flow at $\beta^* = \beta/2\pi = 1/4$, 1/2, 1, 2, 4, 8. (a) Results of direct numerical FV simulation of Eq. (5). (b) Profiles computed from Eq. (13) by using the model given by Eq. (15) for estimating the effective velocity. The arrow indicates increasing values of the flow-to-settling ratio β.

In order to provide a more direct comparison, the computed and predicted profiles at the values $\beta^* = \beta/2\pi = 1/2$ and $\beta^* = 4$ are reported onto a single plot in Fig. 7. The data show that the concentration profile is quantitatively well captured by the model for both values of β. In both cases, the predicted overall tail-to-head concentration jump $\Delta\overline{C}_{ss} = \overline{C}_{ss}(0) - \overline{C}_{ss}(1)$ agrees quantitatively with that obtained by direct numerical FV simulation.

Next, let us analyze in more detail the effective velocity estimate by analyzing the model prediction vs. the actual effective velocity computed from the direct FV simulation by differentiation of Eq. (13).

Fig. 8 shows the estimate provided by Eq. (15) at $\beta^* = 1/2$ (continuous line) and $\beta^* = 2$ (dashed line) for Model **A** flow. The circle and square symbols represent the actual effective velocity computed by numerical differentiation of the direct simulation data at the same values of β^*. Both profiles show the same qualitative trend consisting of a bimodal behavior, with the two maxima

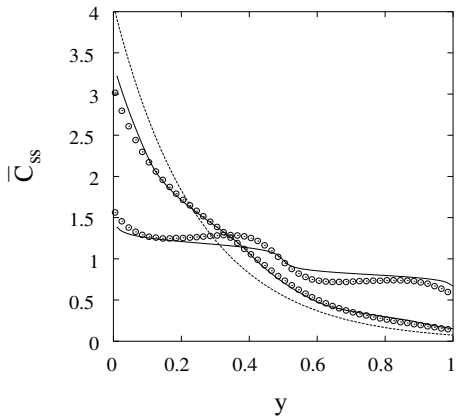

Fig. 7. Comparison of computed (circles) and predicted (continuous lines) steady-state profiles for Model **A** at $\beta^* = \beta/2\pi = 1/2$ and $\beta^* = 4$. The dotted line represents the exponential steady-state profile in the absence of stirring, i.e. at $\beta = 0$.

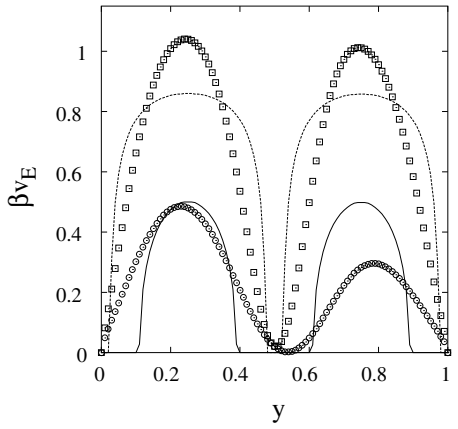

Fig. 8. Comparison of predicted (lines) and computed (symbols) effective velocity for Model **A**. The circles and the continuous line refer to the case $\beta^* = \beta/2\pi = 1/2$. The squares and the dashed line refer to the case $\beta^* = 4$.

approximately located at the center of the two vortices. The main qualitative difference is that the actual effective velocity shows a nonsymmetric profile with respect to $\tilde{y} = 1/2$, whereas the model yields a perfectly symmetric dependence. This discrepancy becomes more relevant al low β-values, i.e. when the action of the stirring field is weak compared to that of the settling bias.

Although widely used in the literature dealing with homogenization dynamics, Model **A** flow is not a solution of a Navier–Stokes boundary value problem. For this reason, it is important to test the validity of the model in more realistic flow situations, such as the creeping flows provided by the cavity problems Model **B** and **C**. Fig. 9 shows the structure of the inflowing–outflowing flux tube (gray shaded area) and of the recirculating loops (white regions) at $\beta = 16$ for Model **B** and Model **C** flows. As can be noticed, in both cases there are $\tilde{y}$-values such that $\sigma_+(\tilde{y}) \neq \emptyset$ (i.e. there are points onto the intersection of the flux tube with Σ such that the vertical component of the

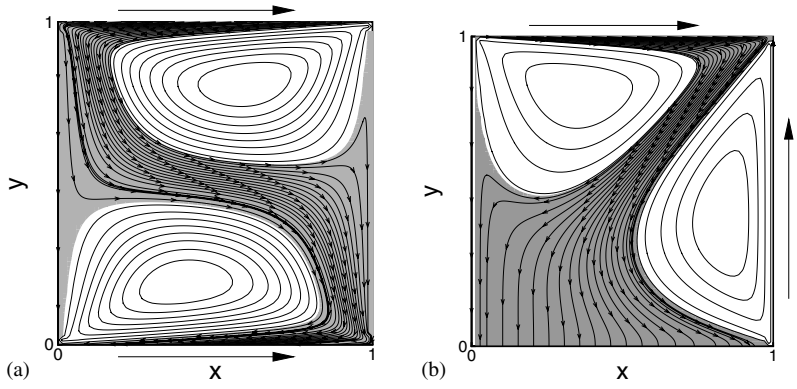

Fig. 9. Structure of the inflowing–outflowing flux tube (gray shaded area) at $\beta = 16$ for Model **B** flow (a), and Model **C** flow (b). Recirculating loops are represented in white.

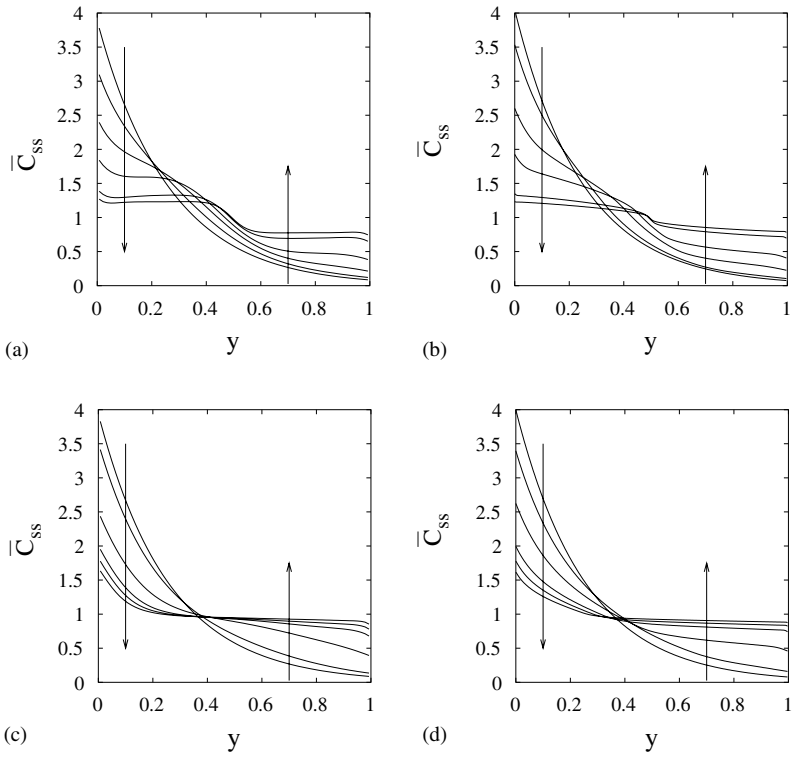

Fig. 10. Comparison of computed and predicted particle concentration profiles for the cavity flow system. (a) Computed profiles for Model **B** flow. (b) Predicted profiles for Model **B** flow. (c) computed profiles for Model **C** flow. (d) Predicted profiles for Model **C** flow. The arrows indicate increasing values of β, $\beta = 4$, 8, 16, 64, 128, and 256.

resulting flow is directed upward). For the CF system, the recirculation loops possess a different geometrical structure with respect to the lobes associated with Model **A** flow.

Fig. 10 shows the comparison between computed and predicted profiles for the two flows. In the case of Model **B** flow (Fig. 10(a) and (b)), the qualitative trend of particle steady-state profile is analogous to what observed in the case of Model **A** flow, and the prediction tends to slightly overestimate the homogenizing action of the stirring flow. Yet, the top-to-bottom concentration difference is well predicted. The profiles associated to Model **C** flow ((Fig. 10(c) and (d)) are qualitatively different with respect to the previous cases (at least at high β-values) in that the steepest concentration gradient is localized in the bottom half of the flow domain. In this case, the prediction agrees quantitatively for the entire profile.

5. Application to a slurry reactor

In this section, we analyze the feasibility of the approach proposed above in predicting vertical stationary profiles of particle concentration inside a baffled stirred vessel under turbulent flow conditions.

5.1. Stirred vessel geometry and numerical techniques

The simulated stirred tank consisted of a vertical, cylindrical, flat-bottomed vessel of equal diameter, T, and height, H ($T = H = 0.154$ m). The vessel was equipped with four vertical baffles of width $W = T/10$ and was closed with a lid. Agitation was provided by a six flat-blade Rushton turbine of diameter $D = T/3$ and off-bottom clearance $C = T/3$. The liquid density and viscosity were $\rho = 1096$ kg/m^3 and $\mu = 1.76$ mPa s, respectively. The impeller rotational speed was set to $N = 13.33$ s^{-1}, thus a fully turbulent flow regime was attained in the vessel ($Re = \rho N D^2/\ \mu = 21\,600$). The three dimensional stirring field was computed by solving the Reynolds Averaged Navier–Stokes equations (RANS) coupled with the standard k–ε turbulence model, as implemented in the commercial CFD code CFX-4.3. As pertains to the impeller simulation strategy, the inner–outer approach was adopted (Brucato et al., 1994) that allows to obtain a fully predictive steady-state velocity field in baffled stirred vessels through the explicit simulation of both the moving impeller and the stationary baffles. The computational grid consisted of 46 080 cells and 7680 cells for the outer and the inner domain, respectively. Thanks to periodicity considerations, the outer and inner domains were limited to $\pi/2$ and $\pi/3$, respectively, and periodic boundary conditions were imposed in the azimuthal direction. Further details on the numerical methods here employed can be found elsewhere (Brucato et al., 1998; Montante et al., 2001). It is worth mentioning that single-phase flow in the stirred vessel geometry considered in this article has been extensively investigated and cross-validated by experiments and CFD simulations. Therefore, the suitability of the selected mathematical models and computational approach in providing reliable results has been already established in the references quoted above.

Two-dimensional vector plots of the flow field onto a vessel cross-section, and a vertical plane through the shaft are represented in Fig. 11. The velocity field structure onto the horizontal cross-section highlights the fourth-fold symmetry stemming from the presence of the baffles, placed symmetrically at $\pi/4$, $3\pi/4$, $5\pi/4$, and $7\pi/4$ in the reference frame of the figure. The structure onto the vertical plane reveals the presence of the typical recirculation loops above and below the impeller.

5.2. Direct numerical simulation of the SVM

Once the stirring field has been computed as described above, the PDE Eq. (5) expressing the time evolution of the three-dimensional particle concentration field in the SVM approximation can be obtained by resorting to numerical discretization. A cylindrical coordinate system with the z-axis directed upward along the vessel axis (i.e. $z = 0$ coincides with the vessel bottom) was used. The variables were made dimensionless by using the vessel height, H, as reference length L, and the impeller tip linear velocity as reference velocity V (see Eq. (4)). The reference concentration, C_{ref} was chosen so as to make unity the overall mass of the dispersed phase. Thus, in this reference frame Eq. (5) writes explicitly as

$$\frac{\partial \tilde{c}}{\partial \theta} = -\beta\left(v_r \frac{\partial \tilde{c}}{\partial \tilde{r}} + \frac{v_\phi}{\tilde{r}} \frac{\partial \tilde{c}}{\partial \phi} + v_z \frac{\partial \tilde{c}}{\partial \tilde{z}}\right) + \frac{\partial \tilde{c}}{\partial \tilde{z}} + \frac{1}{Pe}\left[\frac{1}{\tilde{r}} \frac{\partial}{\partial \tilde{r}}\left(\tilde{r} \frac{\partial \tilde{c}}{\partial \tilde{r}}\right) + \frac{1}{\tilde{r}^2} \frac{\partial^2 \tilde{c}}{\partial \phi^2} + \frac{\partial^2 \tilde{c}}{\partial \tilde{z}^2}\right], \tag{16}$$

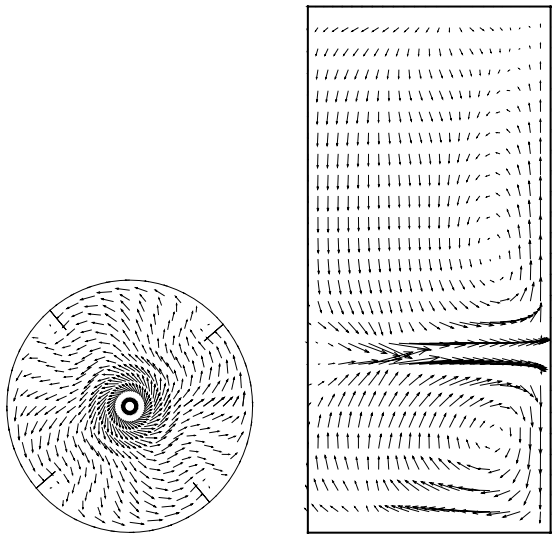

(a) (b)

Fig. 11. Two-dimensional vector plots of the flow inside the vessel. (a) Flow onto the horizontal cross-section at $\tilde{z} = 1/5$. (b) Recirculation loops onto a vertical plane placed symmetrically between two consecutive baffles.

where the dimensionless velocity is represented by $\mathbf{v} = v_r\mathbf{e}_r + v_\phi\mathbf{e}_\phi + v_z\mathbf{e}_z$, and the spatial scaled variable are defined as $\tilde{r} = r/H$ and $\tilde{z} = z/H$.

As a numerical scheme, we used a semi-implicit finite-difference relaxation algorithm (Roache, 1976) for obtaining the steady-state profile, corresponding to values of the flow-to-settling ratio ranging in the interval $1 < \beta < 40$.

The initial condition was set to a uniform particle distribution. The FD discretization of Eq. (16) was advanced in time until steady-state was reached.

Starting form the three-dimensional concentration field, cross-section averaged concentration profiles were obtained by numerical integration onto the generic horizontal cross-section of the vessel. Fig. 14(a) shows the averaged concentration profiles for $\beta = 5$, 10, 20 and 40, as a function of the normalized vertical coordinate $\tilde{z}$. A behavior qualitatively similar to that observed in two-dimensional model flow can be recognized. At high β-values, a steep gradient is found at $\tilde{z} = 1/3$, which represents the location of the impeller. A change of profile convexity is also detectable in the upper region of the vessel ($\tilde{z} < 1/2$) for the curve corresponding to $\beta = 40$.

5.3. Estimate of the effective velocity

The qualitative similarity of vertical profiles resulting from two and three-dimensional stirring flows suggests that an estimate for the effective velocity such as that expressed by Eq. (15) could provide a useful tool for predicting average particle distribution along the axial coordinate. However, in this case the inflowing–outflowing flux tube is three-dimensional, and the determination of the cross-section $\sigma(\tilde{z}) = \sigma_-(\tilde{z}) + \sigma_+(\tilde{z})$ is in general nontrivial. Indeed, in the two-dimensional flows examined before, σ could be determined by solving a one-dimensional

inequality involving the streamfunction Φ (e.g, for all of the model flows considered, it can be showed that σ is the set of points of Σ where $0 < \Phi < 1$).

The extension of this method to the three-dimensional case would require the knowledge of a system of streamsurfaces (Aris, 1962) associated with the resulting flow $\mathbf{u}(\tilde{x},\tilde{y},\tilde{z};\beta) = \beta\mathbf{v}(\tilde{x},\tilde{y},\tilde{z}) - \mathbf{e}_z$, $\mathbf{v}(\tilde{x},\tilde{y},\tilde{z})$ being the unperturbed stirring flow. Given that the flow is generally not axisymmetric, the actual computation of the systems streamsurfaces results impractical.

An alternative (although approximate) approach is to reconstruct the structure of the flux tube by integrating a set of trajectories that originate at the vessel top surface. In point of fact, by flow incompressibility, (almost all of) the trajectories that originate at the vessel top must cross the mixing space and exit the system at the bottom surface. It should be noted, however, that the degree of freedom allowed by the third dimension can make the structure of the flux tube remarkably complicated. In any case, once the inflowing–outflowing streamlines have been determined by integration of the advection equation [2] $\dot{\mathbf{x}} = \mathbf{u}(\tilde{x},\tilde{y},\tilde{z};\beta)$, it is possible to compute their intersection with the vessel cross-section at a generic $\tilde{z}$. Fig. 12 shows the result of this computation with $\beta = 20$ and 40, at planes located at different heights within the vessel. The array of streamlines used to determine the intersections was obtained by computing the trajectories of order 10^5 tracers initially uniformly distributed at the vessel top surface.

In each panel, the regions that are devoid of points represent the intersection of recirculating three-dimensional lobes with the given cross-section. The (nonuniform) distribution of points in the remaining region yields the structure of the intersection of the flux tube with the specified cross-section (ideally, one would need an infinite number of intersections to specify the structure of σ). Starting from this picture, an approximate estimate of σ (and therefore of σ_- and σ_+) can be obtained by a box counting procedure, that is, by subdividing the cross-section Σ into nonoverlapping boxes, and by counting the fraction of boxes that contain at least one intersection. A result of this computation for a number of boxes of order 10^4 is presented in Fig. 13. Clearly, there is a upper and a lower threshold for the box size. The upper threshold is dictated by the smallest structure of the flux tube, whereas the lower threshold is related to the overall number of intersections and thus, in turn, by the overall number of particles used for reconstructing the structure of the flux tube.

Once, the measure of the regions σ_- and σ_+ has been determined, the vertical concentration profiles can be computed in closed-form.

Fig. 14(b) shows the particle profiles at different β-values obtained with the estimate of flux tube cross-section described above. The comparison with the FD direct simulation data of Fig. 14(a) shows a good quantitative agreement, especially when the overall concentration jump is considered.

Likewise the two-dimensional cases already examined, the comparison of computed and estimated quantities becomes less quantitative when the effective velocity itself is considered in place of the cross-section averaged concentration. Fig. 15 shows the comparison between actual and estimated effective velocity at different β-values. While the overall bimodal behavior of the estimate is correctly predicted, the estimate of effective velocity derived through geometric arguments

[2] In performing the integration, the discrete set of nodal velocities resulting from the CFD computation was interpolated using a standard trilinear scheme, which yields a globally continuous velocity field.

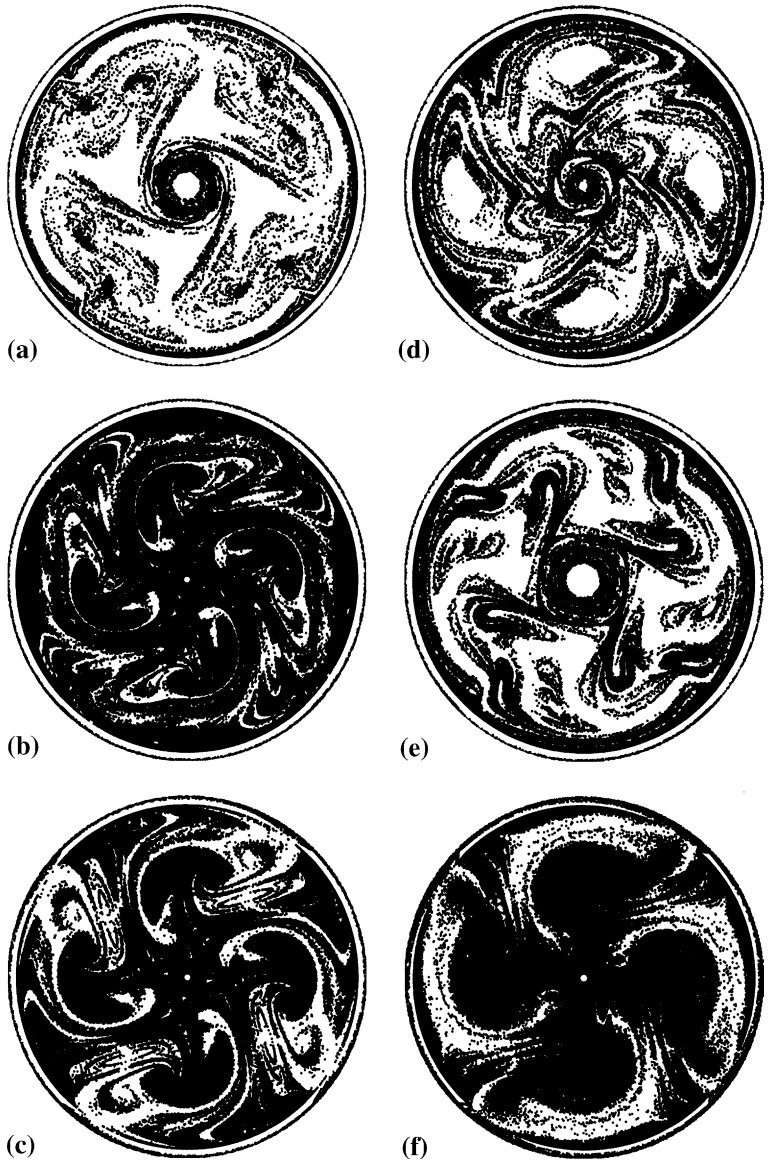

Fig. 12. Structure of the inflowing–outflowing flux tube onto selected cross-sections of the stirred vessel. The black dots represent the intersection of the trajectories of particles that were initially uniformly distributed at the top surface of the vessel. The left and right columns refer to values of the flow-to-settling parameter $\beta = 20$ and 40, respectively. The location $\tilde{z} = z/H$ (H being the vessel height) of the cross-sections are as follows: (a) $\tilde{z} = 0.1$; (b) $\tilde{z} = 0.2$; (c) $\tilde{z} = 0.7$; (d) $\tilde{z} = 0.2$; (e) $\tilde{z} = 0.7$; (f) $\tilde{z} = 0.9$.

appears less smooth than the actual effective velocity profile. Also, at low values of the flow-to-settling parameter β, the model overpredicts the magnitude of the effective velocity.

In conclusion, the application of the proposed model to a concrete example of industrial flow shows the same level of accuracy than that pertaining to simple two-dimensional model flows.

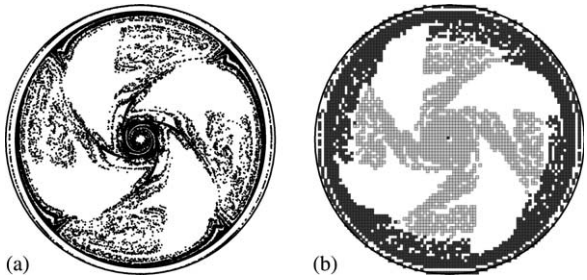

Fig. 13. Numerical computation of the inflowing–outflowing flux tube cross-section area. (a) Intersection of flux lines with an horizontal cross-section. (b) Computation of the flux tube cross-section through box-counting. The dark grey and light grey boxes represent regions of the flux tube where the vertical (i.e. axial) velocity is directed downward and upward, respectively.

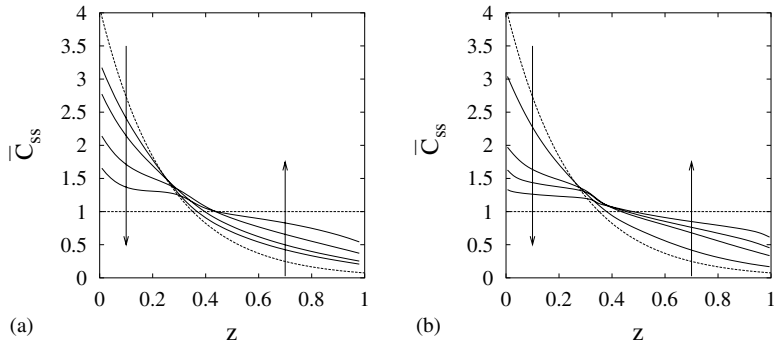

Fig. 14. Comparison of computed (a), and predicted (b) cross-section averaged concentration profiles. Continuous lines concentration profiles at $\beta = 5$, 10, 20 and 40. The dotted lines represent the exponential and uniform profiles associated with the limits $\beta = 0$ and $\beta \to \infty$, respectively. The arrows indicate increasing β-values.

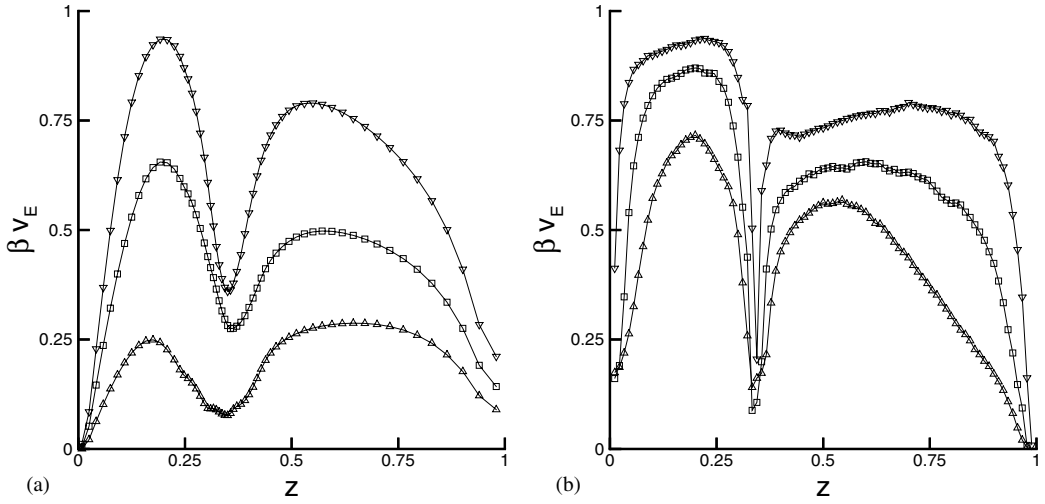

Fig. 15. Comparison of computed (a), and predicted (b) effective velocity profiles. (Δ) $\beta = 10$, ($\square$) $\beta = 20$, and (∇) $\beta = 40$.

6. Concluding remarks

In this article, we develop a geometric approach for estimating vertical (cross-section averaged) concentration profiles of weakly inertial particles stirred by a closed incompressible flow. The mathematical paradigm used for developing the approach is the settling velocity model, which assumes that inertial particle behave as a passive tracer advected by the flow resulting from the stirring field plus a constant vector field expressing the inertial contribution to the particle motion (settling velocity).

Starting from the high dimensional (i.e. two or three-dimensional) setting of the SVM, the one-dimensional equation expressing the cross-section averaged particle concentration profile is derived. This equation is not closed in that it contains an integral term expressing the correlation between the vertical (i.e. parallel to the settling direction) component of the stirring field, and the concentration variation onto the given cross-section. An estimate based on geometric arguments is provided for this term. The estimate, based on the structure of the flow resulting from the superposition of the stirring flow plus the settling contribution, is fully predictive meaning that it does not contain adjustable parameters. It is based on the observation that incompressibility of the resulting flow allows to decompose the flow domain into two disjoint regions, namely an inflowing–outflowing flux tube that crosses the mixing space, and a collection of closed recirculation regions that exchange particle with the flux-tube only by diffusion mechanism. The measure of the flux tube cross-section is used for estimating the effective velocity at any given cross-section.

Stemming from the existence of a streamfunction, the practical computation of the flux tube structure is relatively simple in two-dimensional flow. In all of the two-dimensional model flows examined in this work, the model provides a reasonable prediction of the concentration profiles. The quality of the prediction depends on both the flow-to-settling ratio parameter β and the overall structure of the flow.

The application of the approach proposed to a three-dimensional flows is instead more involved, as it is in general nontrivial to obtain a system of streamsurfaces representing the flow. An approximate method for computing the flux tube cross-section is attempted through a box-counting procedure by considering a swarm of passively advected particles that are initially uniformly distributed at the top surface of the flow domain and computing their intersections with the horizontal cross-section of the mixing space. As a concrete example of application of the method to a fully three-dimensional industrial flow, we consider the CFD-computed solution of the turbulent flow occurring in a baffled cylindrical vessel stirred by a six-blade Rusthon turbine.

The method proposed proves useful to predict qualitatively (and in some cases, quantitatively) the cross-section averaged vertical profiles, both in two and three-dimensional flows. In all of the cases examined, the model tends to overpredict the action of the stirring field, thus yielding more homogeneous profiles than those obtained by direct numerical simulation.

In more general terms, the approach proposed in this paper can be considered as an attempt of connecting the mechanisms of particle dispersion with the geometric structure of a mean stirring field. In particular, the identification of the inflowing–outflowing flux tube and of the recirculating loops can be used as a diagnostics for a semi-quantitative estimate of particle mixing, and allows to single out the impact of the stirring field upon particle homogenization.

References

Aris, R., 1962. Vectors Tensors and The Basic Equation of Fluid Mechanics. Prentice-Hall, Englewood Ciffs, NJ.

Barresi, A., Baldi, G., 1987. Solid suspension in an agitated vessel. Chem. Eng. Sci. 12, 2949–2956.

Brucato, A., Ciofalo, M., Grisafi, F., Micale, G., 1994. Complete numerical simulation of flow fields in baffled stirred vessels: the inner–outer approach. In: IChemE Symposium Series, vol. 2. pp. 155–162.

Brucato, A., Ciofalo, M., Grisafi, F., Micale, G., 1998. Numerical prediction of flow fields in baffeld stirred vessels: a comparison of alternative modelling approaches. Chem. Eng. Sci. 53, 3653–3684.

Brucato, A., Ciofalo, M., Grisafi, F., Magelli, F., Micale, G., 1997. On the simulation of solid particle distribution in multiple impeller agitated tanks via computational fluid dynamics. In: AIDIC Conference Series, vol. 2. pp. 287–294.

Brucato, A., Magelli, F., Nocentini, M., Rizzuti, L., 1991. An application of the network of zones model to solids suspension in multiple impeller mixers. Trans. IChemE 69, 43–52.

Childress, S., Soward, A.M., 1989. Scalar transport and alpha-effect for a family of cat's-eye flows. J. Fluid Mech. 205, 99–133.

Fannjiang, A., Papanicolau, G., 1994. Convection-enhanced diffusion for periodic flows. SIAM J. Appl. Math. 54, 333–408.

Harnby, N., Edwards, M.F., Nienow, A.W. (Eds.), 1997. Mixing in the Process Industries. Butterworth–Heinermann, London.

Johansen, S.T., 1991. The deposition of particles on vertical walls. Int. J. Mult. Flow 17, 355–376.

Kudrna, V., Sysova, M., Fort, I., 1986. A probability form of the diffusion equation and its use to describe the distribution of the solid phase particle concentrations in a mechanically agitated charge. Coll. Czech. Chem. Comm. 51, 1910–1922.

Lamb, R.G., 1980. In: Longhetto, A. (Ed.), Atmospheric Planetary Boundary Layer Physics. Elsevier, Amsterdam, p. 173.

Leonard, G.L., Mitchener, M., Self, S.A., 1980. Particle transport in electrostatic precipitators. Atmos. Environ. 14, 1289.

Loth, E., 2000. Numerical approaches for motion of dispersed particles, droplets and bubbles. Progr. Energy Combust. Sci. 26, 161–223.

Magelli, F., Fajner, D., Nocentini, M., Pasquali, G., 1990. Solid distribution in vessels stirred with multiple impellers. Chem. Eng. Sci. 45, 615–6125.

Mann, R., 1986. Gas–liquid stirred systems: towards a unified theory based on the network of zones. Chem. Eng. Res. Des. 64, 23–34.

Maxey, M.R., Riley, J.J., 1983. Equation of motion for a small rigid sphere in a nonuniform flow. Phys. Fluids 26, 883–888.

Micale, G., Montante, G., Grisafi, F., Brucato, A., Godfrey, J., 2000. Inner–outer CFD simulation of particle distribution in stirred vessel. Chem. Eng. Res. Des. 78, 435–444.

Montante, G., Lee, K.C., Brucato, A., Yianneskis, M., 2001. Numerical simulation of the dependency of flow pattern on impeller clearance in stirred vessels. Chem. Eng. Sci. 56, 3751–3770.

Montante, G., Pinelli, D., Magelli, F., 2002. Diagnosis of solid distribution in vessels stirred with multiple PBTs and comparison of two modelling approaches. Can. J. Chem. Eng. 80, 665–673.

Nocentini, M., Pinelli, D., Magelli, F., 2002. Dispersion coefficient and settling velocity in agitated slurry reactor stirred with multiple Rushton turbines. Chem. Eng. Sci. 57, 1877–1884.

Ottino, J.M., 1989. The Kinematics of Mixing. Stretching, Chaos and Transport. Cambridge University Press, Cambridge.

Pinelli, D., Nocentini, M., Magelli, F., 2001. Solids distribution in stirred slurry reactor: influence of some mixer configurations and limits to the applicability of a simple model for predictions. Chem. Eng. Comm. 188, 91–107.

Roache, P.J., 1976. Computational Fluid Dynamics. Hermosa Publishers, Albuquerque.

Reeks, M.W., 1983. The transport of discrete particles in inhomogenoeus turbulence. J. Aerosol Sci. 14, 293–305.

Shirolkar, J.S., Coimbra, C.F.M., Queiroz McQuay, M., 1996. Fundamental aspect of modeling turbulent particle dispersion in dilute flows. Progr. Energ. Combust. Sci. 22, 363–369.

Young, J., Leeming, A., 1997. A theory of particle deposition in turbulent pipe flow. J. Fluid Mech. 340, 129–159.

Zaichik, L.I., 1997. Modelling of the motion of particles in non-uniform turbulent flow using the equation for the probability density function. J. Appl. Mech. 61, 127–133.